SLAC-PUB-2321
May 1979
(T/E)

PRELIMINARY RESULTS FROM THE MARK II DETECTOR

Daniel L. Scharre
Stanford Linear Accelerator Center
Stanford University, Stanford, California 94305

Abstract: Preliminary results from the SLAC-LBL Mark II magnetic detector at SPEAR are presented. Discussed are two-photon production of η' and recent work on ψ and ψ' decays.

Résumé: Nous présentons des résultats préliminaries obtenus à SPEAR à l'aide du détecteur Mark II (SLAC-LBL). Ils consistent en la production du η' par échange de deux photons et en des travaux récents sur certains desintégrations du ψ et du ψ'.

Presented at the XIV Rencontre de Moriond:
Les Arcs, France, March 11-23, 1979

* Work supported by the Department of Energy under contract number EY-76-C-03-0515.

I. Detector

A schematic drawing of the SLAC-LBL Mark II magnetic detector[1] is shown in Figure 1. Starting from the interaction region, the detector consists of two layers of cylindrical scintillation counters around the vacuum pipe,

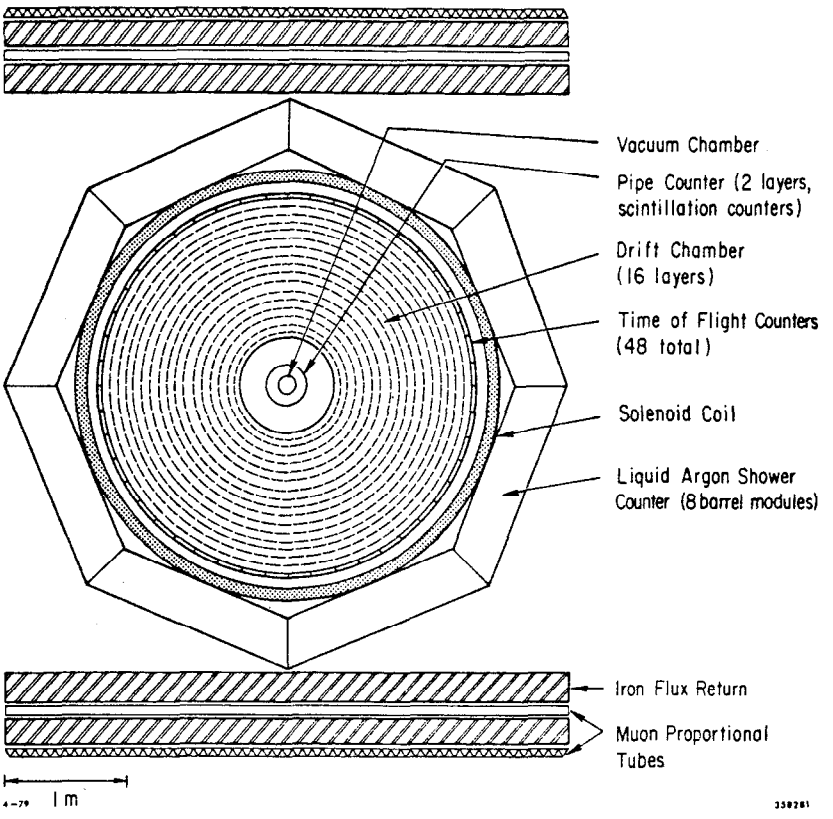

Fig. 1. Schematic drawing of the SLAC-LBL Mark II magnetic detector looking along the beam direction. Not shown are the hadron absorbers and proportional tubes for muon detection along the sides, and the endcap shower detectors.

16 layers of cylindrical drift chambers,[2] 48 time-of-flight (TOF) scintillation counters, an aluminum solenoidal coil which produces a 4.1 kG axial field, 8 lead--liquid argon (LA) shower counters,[3] magnet flux return iron which serves as a hadron absorber, and two planes of proportional tubes for muon detection. In addition, there are shower detectors covering the endcap regions of the detector.

The drift chamber consists of 16 sense wire layers of radii 0.37 m to 1.51 m and provides solid angle coverage out to 85% of 4π sr. The azimuthal coordinates of charged tracks are measured to an rms accuracy of approximately 200 μm at each layer. The polar coordinates are determined from the 10 stereo layers oriented at $\pm 3^{\circ}$ to the beam axis. Figure 2 shows the charged particle rms momentum resolution as a function of momentum. This resolution can be expressed as $\delta p/p = [(0.0145)^2 + (0.005p)^2]^{\frac{1}{2}}$, where p is the momentum in GeV. The first term is the contribution from multiple Coulomb scattering and the second is the contribution from the measurement error.[4] The tracking efficiency is greater than 95% for tracks with $p > 100$ MeV/c over 75% of 4π sr.

The TOF counters provide timing information over 75% of 4π sr. The average flight path is 1.85 m which leads to an average rms resolution of 0.270 ns for Bhabha events. Figure 3 shows the difference between the expected time (based on

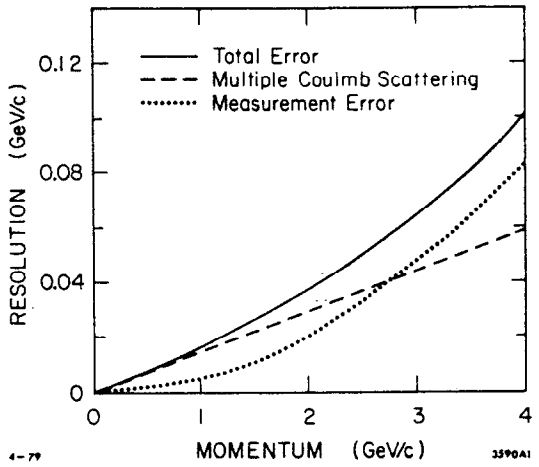

Fig. 2. Charged particle momentum resolution in the drift chamber as a function of momentum.

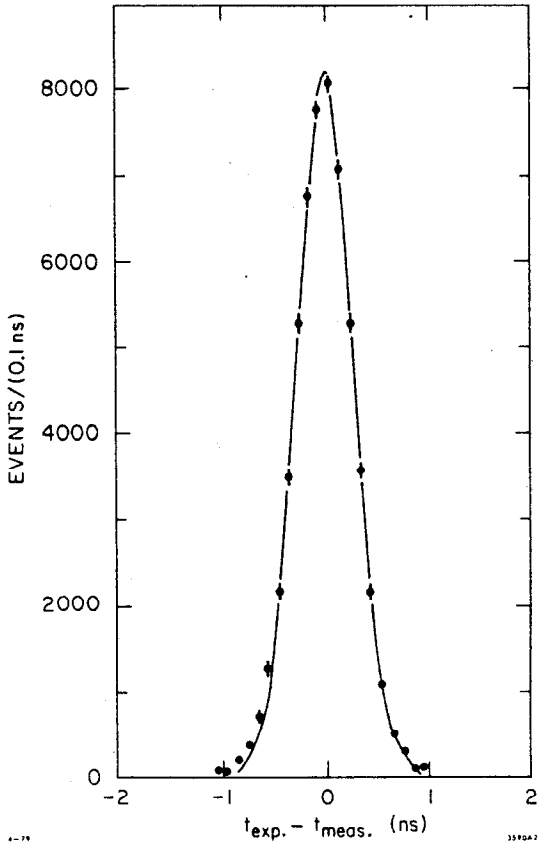

Fig. 3. Expected time minus measured time from the TOF system for a sample of Bhabha events at $E_{cm} = 4.16$ GeV. The curve represents the expected distribution for 0.270 ns resolution.

the measured path length in the drift chamber) and the measured time (from the TOF system) for a sample of Bhabha events at 4.16 GeV center-of-mass energy (E_{cm}). The curve is a Gaussian with $\sigma = 0.270$ ns. For hadrons, the average rms resolution is on the order of 0.300 ns. This leads to a 1-σ separation between π's and K's at 1.35 GeV and between K's and p's at 2.0 GeV.

The shower counter system consists of 8 LA barrel modules around the central detector and two endcap modules. The endcap modules (one liquid argon module and one module consisting of two multi-wire proportional chamber planes) have not been used in any of the analysis which will be discussed. (For the sake of simplicity, all further reference to the shower counter system will refer to the LA barrel module system.) The barrel modules each consist of about 14 radiation lengths of lead and argon, with readout strips parallel, perpendicular to, and at 45° to the beam axis. This system covers approximately 73% of 4π sr. The rms angular resolution obtained for electromagnetic showers is typically 8 mrad both in azimuth and dip angle. The rms energy resolution for photons and electrons is approximately $\delta E/E = 0.12\,E^{-\frac{1}{2}}$, where E is the energy GeV. Figure 4 shows the energy deposited in the liquid argon shower counter system for a sample of Bhabha events at $E_{cm} = 4.16$ GeV. The curve is a Gaussian resolution function (with $\delta E/E = 0.116\ E^{-\frac{1}{2}}$) convoluted with the radiative tail. Figure 5 shows the deposited energy for a sample of low energy electrons (obtained from converted photons in the vacuum pipe and pipe counter). The electrons range in energy from 125 to 175 MeV, and the curve is the expected distribution for $\delta E/E = 0.11\ E^{-\frac{1}{2}}$. In both

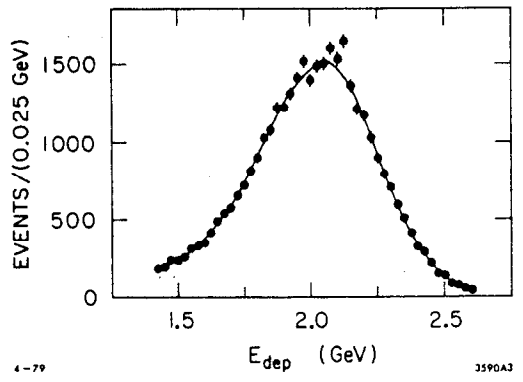

Fig. 4. Energy distribution in the LA barrel module system for a sample of Bhabhas at $E_{cm} = 4.16$ GeV. The curve represents the expected distribution for 0.270 ns resolution.

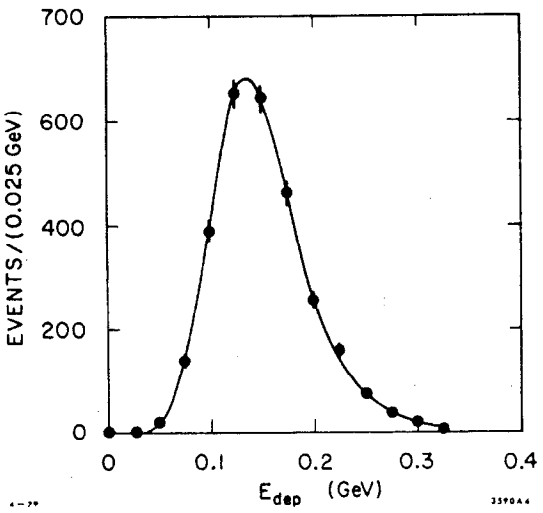

Fig. 5. Energy distribution in the liquid argon barrel module system for a sample of low energy (125 to 175 MeV) electrons. The curve is the expected distribution assuming $\delta E/E = 0.11\, E^{-\frac{1}{2}}$.

figures, the energy collected in the argon has been corrected for collection efficiency, energy loss prior to entering the LA module, and leakage of energy out the back of the module.

Figure 6 shows the detection efficiency for γ's in the LA barrel module system

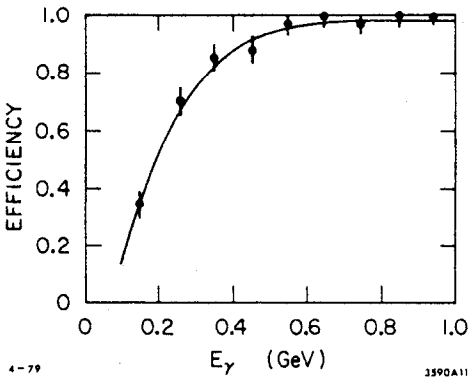

Fig. 6. Detection efficiency for γ's as a function of energy in the LA barrel modules. Data points are measured values, curve is Monte Carlo calculation.

as a function of energy. Geometric acceptance is not included in the efficiency. The data points are obtained by making 2-C fits to 2 and 4 prong events at the ψ according to the hypotheses $\psi \to \pi^+\pi^-\gamma(\gamma)$ or $\psi \to \pi^+\pi^-\pi^+\pi^-\gamma(\gamma)$, where only one γ is used in the fit, and the $\gamma(\gamma)$ system is required to have the mass of the π^o. The efficiency is defined to be the fraction of events in which the missing γ is observed and tracked in the liquid argon (assuming the predicted direction places the missing γ in one of the barrel modules). To reduce background from fake γ's (γ's which are constructed by the software as a result of noise in the shower counter system), only γ's with energy greater than 300 MeV are used in the fits. The curve represents a Monte Carlo analysis of the γ efficiency employing the EGS electromagnetic shower development code.[5)]

Figure 7(a) shows the $\gamma\gamma$ invariant mass distribution for a sample of events at the ψ. Each γ is required to have momentum greater than 150 MeV/c to reduce the fake photon background. A π^o peak is clearly seen, but there is no evidence

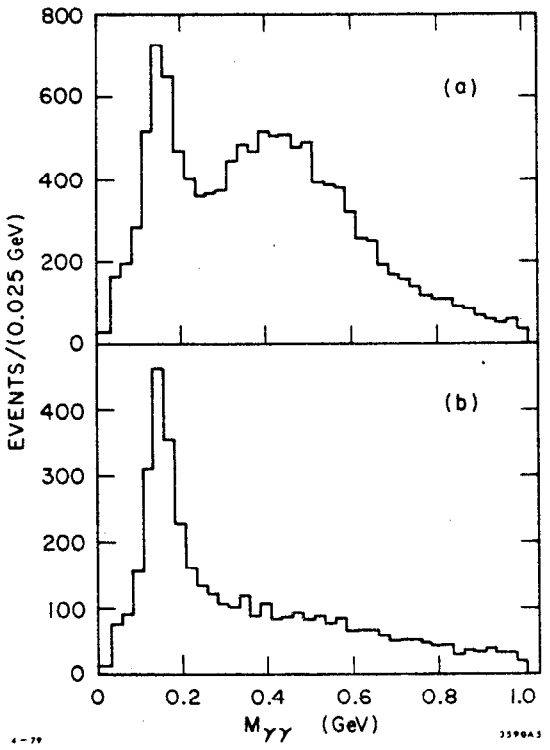

Fig. 7. $\gamma\gamma$ invariant mass distribution for a sample of ψ events.
(a) All combinations with $p_\gamma > 150$ MeV/c,
(b) Same as (a) with the additional requirement that $p_{\gamma\gamma} > 500$ MeV/c.

for η^0 production. (Due to the γ energy distribution, the $\gamma\gamma$ invariant mass distribution tends to peak in the η^0 mass region, making separation of a signal from the background difficult.) Figure 7(b) shows the same distribution after imposing a 500 MeV/c momentum cut on the total momentum of the $\gamma\gamma$ pair.

The π^0 and η^0 detection efficiencies as functions of momentum are shown in Figure 8. In the efficiency calculation, geometric acceptance is included (At the time of the analysis, only seven of the eight LA barrel modules were operational), and in the case of the η^0, the branching fraction into $\gamma\gamma$ is also included. The solid curves are the Monte Carlo predictions. The three data points are measured π^0 efficiencies. These efficiencies are calculated by comparing the number of 1-C fits to the decays $\psi \to \pi^+\pi^-(\pi^0)$ and $\psi \to \pi^+\pi^-\pi^+\pi^-(\pi^0)$ to the number of 5-C fits to the same decays, where the π^0 is observed.

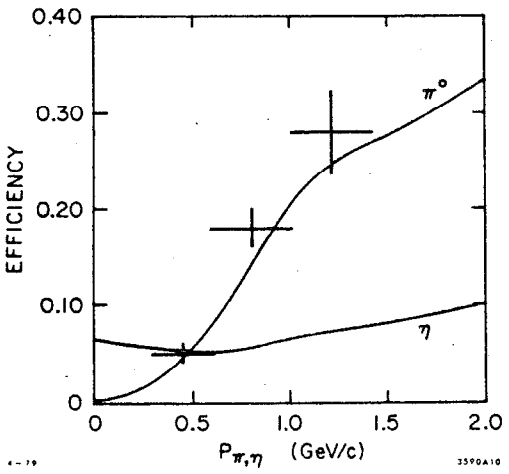

Fig. 8. π^0 and η^0 detection efficiencies as functions of momentum. Geometry (for seven LA barrel modules) and branching fractions are included. Data points are measured π^0 values; curves are Monte Carlo calculations.

The detector is triggered with a two-stage hardware trigger,[6] selecting (with efficiency greater than 99%) all interactions emitting at least one charged track within 75% of 4π sr and another track within 85% of 4π sr. The luminosity is measured with independent shower counters detecting Bhabha scattering at 22 mrad, and checked against wide-angle Bhabha events observed in the central detector.

II. Two-Photon Production

Although two-photon production is generally considered as a background to the simpler annihilation events in e^+e^-, there has been much recent work, both

theoretical and experimental, devoted to the analysis of two-photon production. The basic diagram is shown in Fig. 9. The final state consists of the scattered electron and positron (in general at small angles to the beam axis) and hadrons (or lepton pairs) created from the virtual photon pair. We have observed evidence for η' production in the reaction

$$e^+e^- \rightarrow e^+e^- \eta' \ . \qquad (1)$$

The final state electron and positron are not observed. The η' is observed in the central detector decaying into $\rho\gamma$.

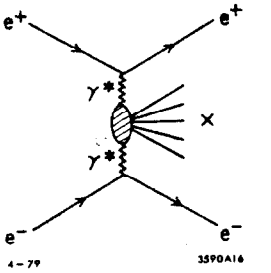

Fig. 9. Diagram for two-photon production.

The data sample consists of data taken by the Mark II at center-of-mass energies between 4.42 and 7.4 GeV. The total integrated luminosity is 5640 nb^{-1}. Events are selected which have only two oppositely charged tracks coming from the interaction region and only one γ detected in the LA barrel modules. Events with charged tracks which are identified as particles other than pions are eliminated. The difference between the measured and expected TOF (based on the pion hypothesis) is required to be less than three standard deviations of the measured resolution; the deposited energy in the liquid argon is required to be consistent with the pion hypothesis (to eliminate electrons); and it is required that there be no track-associated hits in the muon chambers. A γ energy cut of $E_\gamma > 170$ MeV is applied to reduce background from fake γ's, and γ's within 60 cm (at the shower counter radius) of either charged track are ignored in order to reduce backgrounds from interacting charged tracks and from pattern recognition ambiguities.

Background from e^+e^- annihilation is reduced by requiring that the transverse momentum of the $\pi^+\pi^-\gamma$ state about the beam axis be less than 250 MeV/c, and that the acoplanarity angle between the di-pion system and the γ be less than 0.5 rad (0. rad is back-to-back when projected onto the plane normal to the beam axis). The contribution from lepton or pion pairs produced in two-photon interactions combined with fake photons is suppressed by requiring that the transverse momentum of the di-pion system be greater than 50 MeV/c and the acoplanarity angle between the π's be greater than 0.05 rad. Sixty-nine events fulfill these requirements. They have been visually scanned and seven were rejected because there were ≥ 4 aligned digitizations in the inner layers of the drift chamber, indicating an additional unrecognized small angle charged track.

The $\pi^+\pi^-\gamma$ invariant mass distribution for the final sample of events, given in Figure 10, shows a clear η' signal. The mass resolution is consistent with expectations. No cut has been made on the $\pi^+\pi^-$ invariant mass, but it has been verified that the $\pi^+\pi^-$ mass distribution is compatible with all pairs coming from ρ^0 decays for the subsample of events lying in the η' mass region (defined as $0.8 < M_{\pi\pi\gamma} < 1.1$ GeV).

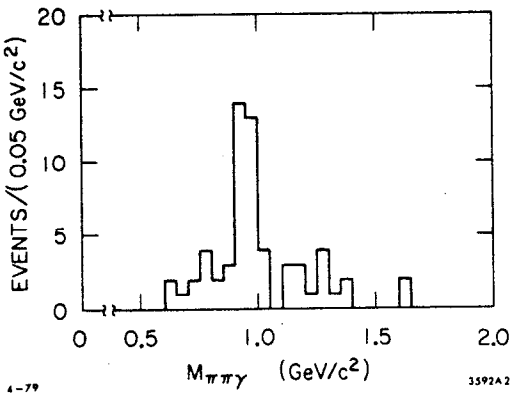

Fig. 10. $\pi^+\pi^-\gamma$ invariant mass distribution for sample of two-photon events.

Figure 11 shows the transverse momentum ($p_\perp$) distribution for events in the entire data dample. The shaded region represents those events in the η' mass region. The η' events occur mainly at low transverse momenta in contrast with the background events. The solid curve shows the expected $p_\perp$ distribution for the two-photon process, normalized to the observed number of η' events.

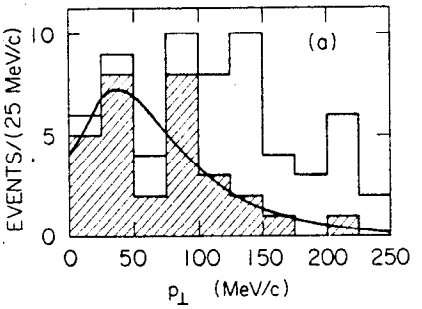

Fig. 11. Transverse momentum distribution for all events. Shaded region are those events in the η' mass region.

The background from e^+e^- annihilation events is studied using multihadron events. $\pi^+\pi^-\gamma$ invariant mass combinations are calculated regardless of the existence of additional charged tracks or γ's, but keeping all other criteria in the event selection. No peaking in the mass distribution is observed. Analysis of the $p_\perp$ distribution for these events shows it to be nearly uniform.

Table I shows the measured cross section for reaction (1) as a function of E_{cm}. The background was subtracted using events in the adjacent mass regions. The detection efficiency was determined by a Monte Carlo simulation using the cross section calculation and angular distribution of Ref. 7. (The branching fraction for $\eta' \to \rho\gamma$ used in the calculation was 0.298 ± 0.017.)

TABLE I: Cross section for $e^+e^- \to e^+e^-\eta'$ as a function of E_{cm}.

E_{cm} (GeV)	$\int \mathscr{L} dt$ (nb^{-1})	Number of Events	σ (nb)
4.42	800	5.1 ± 2.6	0.98 ± 0.50
4.5 - 5.0	2130	4.3 ± 2.6	0.30 ± 0.18
5.0 - 6.0	1730	10.3 ± 3.6	0.91 ± 0.32
7.4	980	3.1 ± 2.2	0.84 ± 0.60

The cross section for reaction (1) is directly proportional to the radiative width $\Gamma_{\eta' \to \gamma\gamma}$.[8] Using the two-photon cross section calculation in Ref. 7, we determine $\Gamma_{\eta' \to \gamma\gamma} = 5.9 \pm 1.6$ keV. (The error is statistical only and does not include an estimated systematic error of ±20%.) Using the measured BR($\eta' \to \gamma\gamma$) = 0.020 ± 0.003, the total width is determined to be $\Gamma_{tot} = 300 \pm 90$ keV.[9] The radiative width of the η' is of interest theoretically as predictions for the width vary greatly depending on the quark charges used in the model.[10] Quark models with

fractionally charged quarks and a small pseudoscaler octet - singlet mixing angle lead to the prediction $\Gamma_{\eta' \to \gamma\gamma} \approx 6$ keV under the assumption of equal singlet and octet couplings. The corresponding width for integrally charged quarks is approximately 26 keV.

III. Direct γ Production at the ψ

We present preliminary results on inclusive γ production at the ψ. Rather than using γ's detected in the shower counter, γ's which convert in the $0.06 - X_o$ vacuum pipe and pipe counter are used in the analysis. Although the statistics are poorer than would be obtained using γ's in the shower counter, there are three advantages to using this method. First, the energy resolution is much better than that obtained with γ's in the liquid argon since it depends on the momentum resolution for charged tracks in the drift chamber. Second, the trigger efficiency can be estimated very well since essentially all converted γ's which are observed in the central detector will provide a trigger. Thus, the detection efficiency is merely a geometric problem. Third, there is no problem with misidentification of high energy π^o's as γ's because of shower overlap in the LA barrel modules.

Of particular interest is the direct production of γ's (i.e., γ's which do not originate from the decays of hadrons such as π^o's or η^o's). Most hadronic decays of the ψ proceed via three gluons as shown in Fig. 12(a).[11] However, one can replace one of the final-state gluon lines by a photon, resulting in the diagram shown in Figure 12(b). The resulting width is smaller by a factor proportional to α/α_s, where α_s is the strong-coupling constant and α is the fine-structure constant. Using a value for $\alpha_s = 0.19$, one obtains the result

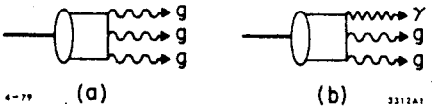

Fig. 12. (a) Diagram for ψ decays via three-gluons. (b) ψ decay diagram where one gluon line has been replaced by a γ.

$\Gamma(\psi \to \gamma gg)/\Gamma(\psi \to ggg) \approx 0.12$.[12] Taking into account other hadron decays and decays into lepton pairs, $\Gamma(\psi \to \gamma gg)/\Gamma_{tot} \approx 0.09$. Although the width is relatively small, the inclusive production cross section rises with x (defined as the γ momentum divided by the beam energy), whereas background from hadronic decays falls with x. Thus, one expects to see an excess of γ's at large x. The expected inclusive γ distribution as a function of x is shown in Figure 13. The presence of resonance

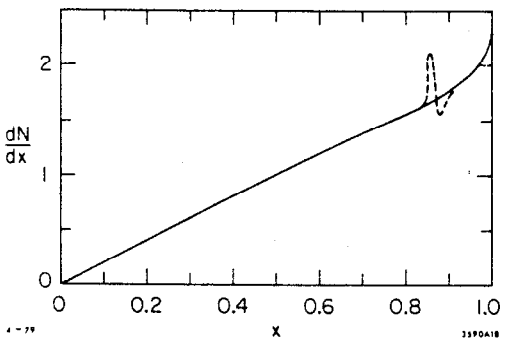

Fig. 13. Theoretical inclusive distribution of direct γ's as a function of x (scale is arbitrary).

structure in the final state is expected to perturb the distribution as shown by the dashed curve, although the area under the distribution is expected to be invariant by the usual duality arguments.

The data used in this preliminary analysis consists of approximately 400,000 produced ψ's. In the final analysis, we expect to increase the data sample by a factor of 2 - 3. Figure 14(a) shows the measured inclusive γ distribution as a function of x. The large x region is shown expanded in Figure 14(b). Clear peaks are seen in the x distribution corresponding to the decay $\psi \to \eta'\gamma$ (at x=0.90) and the background QED process $e^+e^- \to \gamma\gamma$ (at x=1.00). After eliminating most of the QED events and correcting the distribution for acceptance, the resulting distribution is shown in Figure 15.

Ideally, in order to measure the direct γ production, one would measure the inclusive π^o and η^o production distributions, and use these distributions to predict the γ distribution originating from hadronic decays. The difference between the measured and predicted distributions would give the direct γ distribution. This analysis has not yet been done, as good measurements of π^o and η^o spectra are not available. A preliminary prediction of the background from hadronic decays based on unpublished data from the Lead-Glass Wall experiment at SPEAR[13] is shown as the solid curve in Figure 15. The dashed curves represent the estimated error in the prediction. Unfortunately, data is not available above x = 0.6, because of lack of statistics in the Lead-Glass Wall analysis.

A straight-line extrapolation of the prediction at low x to large x shows an excess in the γ spectrum at large x. However, due to the preliminary stage of the analysis, only rather conservative limits,

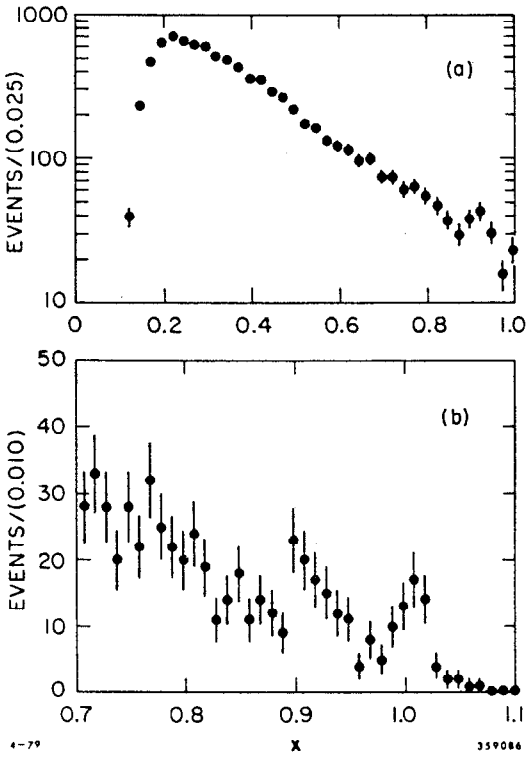

Fig. 14. Uncorrected inclusive γ distribution as a function of x for converted γ's at the ψ for (a) all events, and (b) events with x > 0.7.

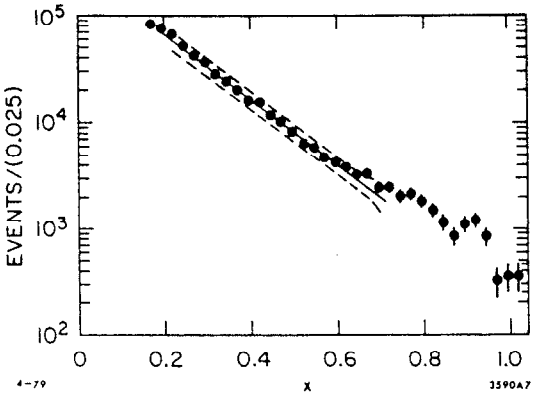

Fig. 15. Inclusive γ distribution at the ψ corrected for acceptance and detection efficiency. Curves are described in text.

which do not depend upon an understanding of the background, will be given for the branching fraction. An upper limit can be set based on the assumption that there is no background from hadronic decays above $x = 0.8$ (i.e., all observed γ's are direct). After correcting for the expected $1+\cos^2\theta$ distribution at large x [12] (the acceptance corrections applied to the data assumed isotropic production of γ's), and for the fraction of the distribution below $x = 0.8$, one obtains $\Gamma(\psi \to \gamma gg)/\Gamma_{tot} \lesssim 0.054$. This limit is already smaller than the predicted branching fraction by nearly a factor of 2. However, there is some uncertainty as to the correct value of α_s to use.[14] Values of α_s which predict a branching fraction consistent with this number are not inconsistent with some theoretical models which describe the charmonium spectrum.

A lower limit on this branching fraction can be set by summing the branching fractions for the measured exclusive final states which have been observed: $n\gamma$, $\eta'\gamma$, and $f\gamma$.[15] Correcting this number for the fraction of the distribution with $x < 0.8$, a lower limit of $\Gamma(\psi \to \gamma gg)/\Gamma_{tot} \gtrsim 0.016$ is obtained.

IV. Exclusive Decays of $\psi \to \pi^+\pi^-\gamma\gamma$

A sample of ψ events (described in the previous section) containing two charged prongs and at least two γ's observed in the LA barrel modules were fit to the hypothesis $\psi \to \pi^+\pi^-\gamma\gamma$. Events with charged tracks identified as particles other than pions were eliminated. Events with more than two γ's were multiply fit for each pair of γ's. This was to prevent loss of events with extra fake photons. No constraint was made on the $\gamma\gamma$ invariant mass. Events consistent with the following decay modes were observed.

$$\psi \to \eta' \gamma \quad (2)$$
$$\qquad\quad \hookrightarrow \pi^+\pi^-\gamma$$

$$\psi \to \rho^0 \pi^0 \quad (3)$$
$$\qquad\quad \hookrightarrow \pi^+\pi^-$$

$$\psi \to \rho^\pm \pi^\mp \quad (4)$$
$$\qquad\quad \hookrightarrow \pi^\pm \pi^0$$

$$\psi \to \pi^+\pi^-\pi^0 \quad \text{(non-resonant)} \quad (5)$$

The $\gamma\gamma$ invariant mass distribution is given in Figure 16(a), showing a clean π^0 peak. The $\pi^+\pi^-$ invariant mass distribution is shown in Figure 16(b). The recoiling γ's are required to form a π^0 ($0.12 < M_{\gamma\gamma} < 0.15$ GeV), and events with charged ρ's ($0.60 < M_{\pi^\pm\pi^0} < 0.90$ GeV) are eliminated. A ρ^0 peak is clearly seen here.

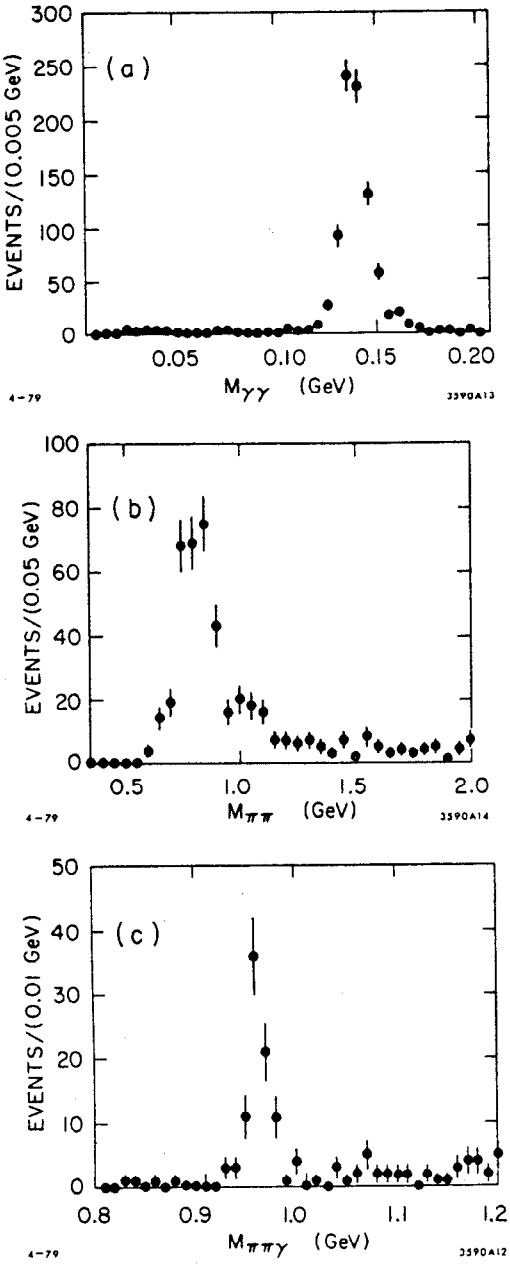

Fig. 16. Invariant mass distribution for a sample of events which fit $\psi \to \pi^+\pi^-\gamma\gamma$. (a) $\gamma\gamma$ mass. (b) $\pi^+\pi^-$ mass recoiling against a π^o with events with $\rho^\pm$ candidates eliminated. (c) $\pi^+\pi^-\gamma$ mass, with events containing a π^o eliminated. Cuts are described in detail in the text.

Finally, an η' peak is observed in Figure 16(c) showing the $\pi^+\pi^-\gamma$ invariant mass distribution (with π^o events eliminated). In all cases, the invariant masses are calculated using the fitted values of the track parameters.

The resulting branching fractions are given in Table II and compared to previously published values. The $\rho\pi$ branching fractions are consistent with previous measurements, but the $\eta'\gamma$ branching fraction is somewhat larger (but see Ref. 15). The branching ratio to 3π (including $\rho\pi$) is measured to be $BR(\psi \to \pi^+\pi^-\pi^o) = 0.0140 \pm 0.0020$. This final state is observed to be nearly all $\rho\pi$, with $\Gamma(\rho\pi)/\Gamma(3\pi) = 0.94 \pm 0.06$.

V. ψ' Cascade Decays

Although considerable work has been done on analyzing the states arising from radiative decays of the ψ and ψ',[20] the connection between the observed states and the predicted charmonium levels are still unclear in many cases. Figure 17 shows the expected low-lying charmonium levels with their associated quantum numbers. The solid lines

TABLE II. Measured Branching Fractions for $\psi \to \rho\pi$ and $\psi \to \eta'\gamma$.

Decay Mode	This Measurement	Previous Measurements
$BR(\psi \to \eta'\gamma)$	$3.4 \pm 0.7 \times 10^{-3}$	$3.8 \pm 1.3 \times 10^{-3}$ a) $2.2 \pm 1.7 \times 10^{-3}$ b) $2.4 \pm 0.7 \times 10^{-3}$ c)
$BR(\psi \to \rho\pi)$	0.0132 ± 0.0021	0.010 ± 0.002 c) 0.012 ± 0.003 d) 0.013 ± 0.003 e)
$\Gamma(\rho^o\pi^o)/\Gamma(\rho^\pm\pi^\mp)$	0.56 ± 0.06	0.63 ± 0.22 c) 0.59 ± 0.17 e)

a) This experiment, as measured in the inclusive γ distribution. (See Ref. 15.),
b) Ref. 16, c) Ref. 17, d) Ref. 18, e) Ref. 19.

indicate well established transitions, the ψ and ψ' are unambiguously identified with the vector meson (^3S) levels. The association of the ^3P levels with the χ states is fairly certain. Radiative decays to and from these states and hadronic decays of these states have been observed. However, neither the pseudoscaler partner of the ψ or the ψ' has been established. For the η_c' (the pseudoscaler partner of the ψ'), there are two candidates. A state with mass 3.455 GeV has been observed by the Mark I collaboration[21] in cascade decays of the form

$$\psi' \to \gamma X \qquad (6)$$
$$\hookrightarrow \gamma\,\psi$$

A state with mass 3.59 GeV has been observed at DORIS.[22] The γ produced in the transition from the ψ' to the state at 3.59 GeV is too low in energy to be observed by the LA shower counters. However, the γ produced in the transition to the state at 3.455 GeV should be observable in the detector.

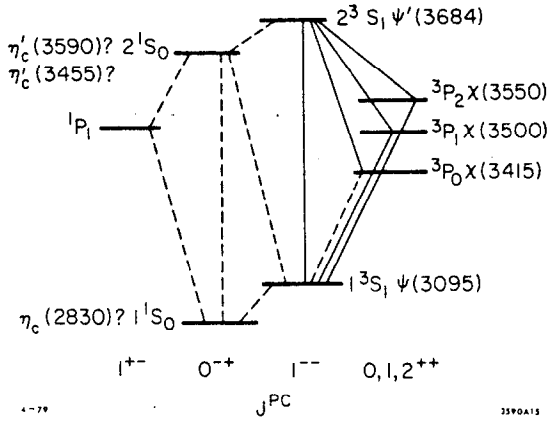

Fig. 17. Diagram of the lowest lying charmonium levels and the associated observed states.

An analysis of the reaction

$$\psi' \to \gamma\,\gamma\,\psi \qquad (7)$$
$$\hookrightarrow \ell^+\,\ell^-$$

is presented. The data sample consists of approximately 250,000 ψ' events. (We expect to have one million events in the final data sample.) The ψ is identified by its decay into lepton pairs. Events with two γ's and two oppositely charged tracks with invariant mass between 2.8 and 3.4 GeV are used in the analysis. A 5-C fit is made to reaction (7) for this sample of events. Figure 18 shows the $\gamma\gamma$ invariant mass for the sample of events with $\chi^2 < 15$. The η^o peak is due to the decay $\psi' \to \eta^o\psi$. These events are eliminated by requiring $M_{\gamma\gamma} < 0.53$ GeV.

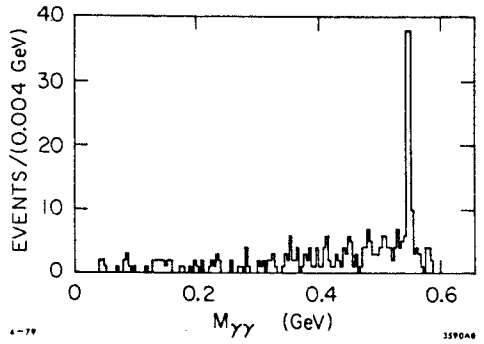

Fig. 18. $\gamma\gamma$ invariant mass distribution for events with $\chi^2 < 15$ for the 5-C fit to reaction (7).

One can construct invariant mass combinations of the ψ with either γ. Previously observed states have shown up in the high-mass combination (with the reflection observable in the low-mass combination). Figure 19 shows the high-mass combination, where peaks associated with the $\chi(3500)$ and $\chi(3550)$ are clearly

visible. No significant peaking is seen in the region of the $\chi(3415)$ or the $\eta_c'(3455)$. Table III shows the number of observed events for each of these intermediate states (after background subtraction) compared to expectations

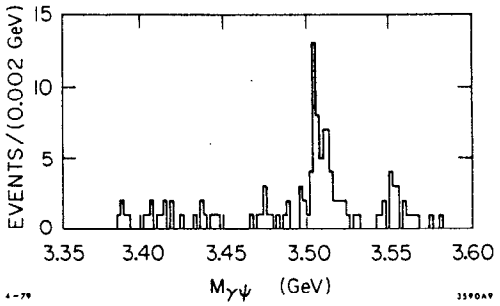

Fig. 19. High-mass $\gamma\psi$ invariant mass distribution for ψ' cascade decays.

based on the measured Mark I branching fractions. (As the efficiency calculations are still preliminary and analysis on the full sample of data will soon be completed, the branching fractions are not presented.) The number of events observed for each of the three χ states is consistent with expectations. However,

TABLE III. Observed Cascade Events Compared to Expected Numbers Based on Measured Branching Fractions.

Transition	Branching Ratio [a]	Number Expected	Number Observed
$BR[\psi' \to \gamma\chi(3550)] \times BR[\chi(3550) \to \gamma\psi]$	0.010	17	20 ± 5
$BR[\psi' \to \gamma\chi(3500)] \times BR[\chi(3500) \to \gamma\psi]$	0.024	64	66 ± 9
$BR[\psi' \to \gamma\chi(3415)] \times BR[\chi(3415) \to \gamma\psi]$	0.002	5	3 ± 3
$BR[\psi' \to \gamma\eta_c'(3455)] \times BR[\eta_c'(3455) \to \gamma\psi]$	0.008	28	0

a) See Ref. 21.

while 28 events are expected at 3455 MeV, no events above background are observed. If one takes the six bins around 3455 MeV, the two observed events lead to a 90% C.L. upper limit of $BR[\psi' \to \gamma\eta_c'(3455)] \times BR[\eta_c'(3455) \to \gamma\psi] < 1.2 \times 10^{-3}$, compared to the measured value of $(8 \pm 4) \times 10^{-3}$ from the Mark I.[21] However, one should be very cautious in interpreting this number. An error on the order of 10 MeV in mass in either of the two experiments would lead to a significant increase in the upper limit.

ACKNOWLEDGMENT

This work was supported by the Department of Energy under contract number EY-76-C-03-0515.

REFERENCES

1. The members of the collaboration are G. S. Abrams, M. S. Alam, C. A. Blocker, A. M. Boyarksi, M. Breidenbach, D. L. Burke, W. C. Carithers, W. Chinowsky, M. W. Coles, S. Cooper, W. E. Dieterle, J. B. Dillon, J. Dorenbosch, J. M. Dorfan, M. W. Eaton, G. J. Feldman, M.E.B. Franklin, G. Gidal, G. Goldhaber, G. Hanson, K. G. Hayes, T. Himel, D. G. Hitlin, R. J. Hollebeek, W. R. Innes, J. A. Jaros, P. Jenni, A. D. Johnson, J. A. Kadyk, A. J. Lankford, R. R. Larsen, V. Lüth, R. E. Millikan, M. E. Nelson, C. Y. Pang, J. F. Patrick, M. L. Perl, B. Richter, D. L. Scharre, R. H. Schindler, R. F. Schwitters, J. L. Siegrist, J. Strait, H. Taureg, M. Tonutti, G. H. Trilling, E. N. Vella, R. A. Vidal, I. Videau, J. M. Weiss, H. Zaccone.
2. W. Davies-White et al., SLAC preprint SLAC-PUB-2181 (1978), to be published in Nucl. Instr. Meth.
3. G. S. Abrams et al., IEEE Trans. on Nucl. Sci. NS-25, 309 (1978)
4. This measurement error is obtained when the tracks are constrained to pass through the known beam position.
5. R. L. Ford, W. R. Nelson, SLAC report SLAC-210 (1978), unpublished.
6. H. Brafman et al., SLAC preprint SLAC-PUB-2033 (1977) unpublished.
7. V. N. Baier, V. S. Fadin, Nuovo Cimento Lett. 1, 481 (1971).
8. S. J. Brodsky, T. Kinoshita, H. Terazawa, Phys. Rev. D4, 1532 (1971).
9. A recent measurement of the η' width in the reaction $\pi^- p \to n$ + missing mass at η' threshold gives $\Gamma_{tot} = 280 \pm 100$ keV. See D. M. Binnie et al., Imperial College, London preprint IC/HENP/79/2 (1979), unpublished.
10. H. Suura, T. L. Walsh, B. L. Young, Nuovo Cimento Lett. 4, 505 (1972).
11. The remaining hadronic decays go through an intermediate photon which couples to a quark-antiquark pair.
12. S. J. Brodsky et al., Phys. Lett. 73B, 203 (1978).
13. An analysis of inclusive γ and π^0 production at the ψ has been done by the Lead-Glass Wall collaboration, but has not been published. The analysis is very similar to the analysis of γ and π^0 production at high energy described in D. L. Scharre et al., Phys. Rev. Lett. 41, 1005 (1978).
14. See discussion in J. D. Jackson, C. Quigg, J. L. Rosner in Proceedings of the Nineteenth International Conference on High Energy Physics, Tokyo, 1978, p. 391.
15. The branching fraction for $\psi \to f\gamma$ has been measured to be $(2.0 \pm 0.3) \times 10^{-3}$ [see G. Alexander et al., Phys. Lett. 72B, 493 (1978)]. Published measurements for $\psi \to \eta\gamma$ are $(0.80 \pm 0.18) \times 10^{-3}$ (see Ref. 16) and $(1.3 \pm 0.4) \times 10^{-3}$ [see W. Bartel et al., Phys. Lett. 66B, 489 (1977)]. There is some controversy over the branching fraction for $\psi \to \eta'\gamma$. Previous measurements are $(2.2 \pm 1.7) \times 10^{-3}$ (see Ref. 16) and $(2.4 \pm 0.7) \times 10^{-3}$ (see Ref. 17). A Mark II measurement based on the peak in the inclusive γ spectrum described in this section gives a value of $(3.8 \pm 1.3) \times 10^{-3}$, and an independent Mark II measurement described in the next section of this talk gives a value of $(3.4 \pm 0.7) \times 10^{-3}$. Finally, a measurement of $(6.1 \pm 1.5) \times 10^{-3}$ was presented by E. Bloom of the Crystal Ball experiment at SPEAR. In the calculation of the lower limit, a value of 6×10^{-3} was used for the sum of these three decay modes.
16. W. Braunschweig et al., Phys. Lett. 67B, 243 (1977).
17. W. Bartel et al., Phys. Lett. 64B, 483 (1976).
18. W. Braunschweig et al., Phys. Lett. 63B, 487 (1976).
19. B. Jean-Marie et al., Phys. Rev. Lett. 36, 291 (1976).
20. See B. H. Wiik, G. Wolf, DESY report DESY 78/23 (1978), unpublished, for a review.
21. J. S. Whitaker et al., Phys. Rev. Lett. 37, 1596 (1976).
22. W. Bartel et al., DESY report DESY 78/49 (1978), unpublished.